FEATURE ARTICLE

Collisions and Chemistry of Super-Excited Molecules: Experiments Using the PUMP−DUMP−PROBE Technique

Marcel Drabbels

Department of Chemistry, Swiss Federal Institute of Technology Lausanne, CH-1015 Lausanne EPFL, Switzerland

Alec M. Wodtke*

Department of Chemistry, University of California at Santa Barbara, Santa Barbara California 93106

Received: March 19, 1999; In Final Form: June 14, 1999

Modern lasers now routinely allow experiments where large populations of highly excited molecules can be prepared with perfect quantum state selection. In a sense, the laser has become the physical chemist's synthetic tool, allowing "optical distillation" of chemical reactants in the most purified form imaginable, individual quantum states. This article describes applications from the authors' laboratory of these methods to studies in chemical reaction dynamics. A detailed description of the PUMP, DUMP, and PROBE technique is presented with specific emphasis on the use of stimulated emission pumping in scattering experiments. Many aspects of the behavior of highly vibrationally excited molecules are presented. These topics include infrared emission, rotational energy transfer, vibrational energy transfer, super-excited molecules colliding with surfaces, and the role of highly vibrationally excited O_2 in the stratosphere.

1. Introduction

A full understanding of how chemical reactions occur must provide knowledge of both the interatomic forces (*interactions*) as well as the atomic and molecular responses to those forces (*dynamics*) as bonds are broken and formed. Armed with such an understanding, we could approach the ultimate goal of the field of molecular reaction dynamics: to be able to predict the outcome of individual chemical events and to model accurately complex systems involving many different elementary reactions. Despite considerable recent advances in experimental and theoretical studies of elementary reactions,[1−4] we are still far from this goal. Theoretical methods have difficulty accurately describing bond formation and cleavage; chemical transition states remain more difficult to characterize than equilibrium structures.[5−7] Future advances in this area are extremely important since it is the nature of the transition state that effectively governs the rates and pathways of chemical reactions.

Particularly relevant to the investigation of the chemical transition state is the study of highly vibrationally excited molecules. Transition states are often characterized by structures dramatically distorted from the equilibrium geometry of either the reactants or the products. Consequently, collisions between molecules in extreme states of distortion and bond extension may exhibit chemical behavior that is particularly sensitive to the nature of the transition state.

On a more practical note, many elementary chemical and photochemical reactions form products with large vibrational energies (hundreds of kJ/mol). Large-amplitude vibrational motion can make it more likely for a chemical reactant to reach the transition state, markedly increasing the reaction rate. Consequently, if we are ignorant of the chemical behavior of super-excited molecules, it may be impossible to model certain important chemical systems.

Much of our understanding about how molecular vibration is related to chemical reactions is based on experiments that measure aspects of the product energy distribution. Nobel Prize winning work using infrared chemiluminescence, laser-induced florescence, and crossed molecular beams scattering have provided much of this kind of information.[8−10] The continued development of high-power lasers has changed the course of this field during the last 10 years. We are no longer restricted to looking at molecular emissions or using the laser as a probe of population distributed among molecular quantum states. Modern lasers now routinely allow experiments where large populations of highly excited molecules can be prepared with perfect quantum state selection. In a sense, the laser has become the physical chemist's synthetic tool, allowing "optical distillation" of chemical reactants in the most purified form imaginable, individual quantum states.

The sheer power of modern lasers has not outshone the ingenuity of the scientists using them. Modern methods of optical pumping go much further than mere quantum state selection.[11−14] The ambitious technical goal of preparing any arbitrary quantum state of any arbitrary molecule will never be reached in a literal sense. On the other hand, for many molecules, we can come close. For these systems, we can treat the reactant quantum numbers as adjustable microscopic reaction conditions to be "dialed in" by the researcher.

This places us in a remarkable position to address many questions regarding the properties of molecules in extreme states of bond extension and distortion. As chemists, we are intrigued

10.1021/jp990972x CCC: $18.00
Published on Web 08/21/1999

by the idea that high vibrational states of reactants can exhibit specific kinds of organized internuclear motion. We wish to know how vibration influences the outcome of chemical reactions, for example, in isomerization,[15−21] atom transfer,[22,23] and dissociative adsorption on solid surfaces.[24]

An issue intertwined with reactivity is molecular energy transfer.[25] Here, we are striving to understand how energy transfer may disrupt the organized internuclear motion mentioned above before reactions can occur. We can now make quantitative measurements of the processes that allow highly vibrationally excited molecules to release their energy, probing the pathways by which they return to thermal equilibrium with their environment. Specific relaxation processes include infrared radiative emission, rotational and vibrational energy transfer to other gas-phase molecules as well as vibrational energy transfer to solid surfaces.

Another important issue concerns excited electronic states. When vibrational energy is comparable to electronic excitation energies, the Born−Oppenheimer approximation can break down and vibration may be converted to electronic energy. Consequently, nonadiabatic curve crossing between electronic states can play an important role for super-excited molecules.[26] Physically, this means that large-amplitude vibrational motion may induce significant electronic reorganization, influencing chemical properties.

All of these questions and many others arise when one considers the properties of super-excited molecules. This paper presents a few highlights from our research showing some examples of the behavior of highly vibrationally excited molecules. Before embarking on this endeavor, we want to stress that this article is not meant to be a review of the field. We apologize in advance for any failure to refer to the enormous quantity of truly inspiring work that has been carried out in the field of chemical reaction dynamics.

The paper is organized as follows. The stimulated emission pumping (SEP) method has been and will continue to be one of the most important experimental methods in this field. Therefore, we present (in section 2) some of the basic principles necessary to understand SEP experiments. In section 3, we turn to the main body of the article, which highlights results from our laboratory using the SEP method. The topics of this section include infrared emission, rotational and vibrational energy transfer, atmospheric chemistry, surface scattering and reactivity, and nonadiabatic electronic coupling in highly vibrationally excited molecules. Section 4 indulges in speculation about the future of the field.

2. Stimulated Emission Pumping

Figure 1 shows an energy level diagram of a specific SEP transition for the illustrative example of nitric oxide, NO, with accurate Morse potentials and wave functions for the $B^2\Pi$ and $X^2\Pi$ states. The sample is excited with a narrowband pulsed laser operating at the "pump" frequency, ω_{pump}, out of thermally populated states into an excited electronic state. A second pulsed laser, tuned to ω_{dump}, stimulates emission out of the excited electronic state transferring population back to a single highly vibrationally excited quantum level in the ground electronic state.

In NO, the PUMP step promotes a bonding electron to an antibonding orbital. Consequently, in the excited state, the equilibrium bond length is greatly extended and the Hooke's Law force constant is reduced. The fundamental quantity governing the probability of vibrational quantum number changes in electronic transitions is the square of the overlap

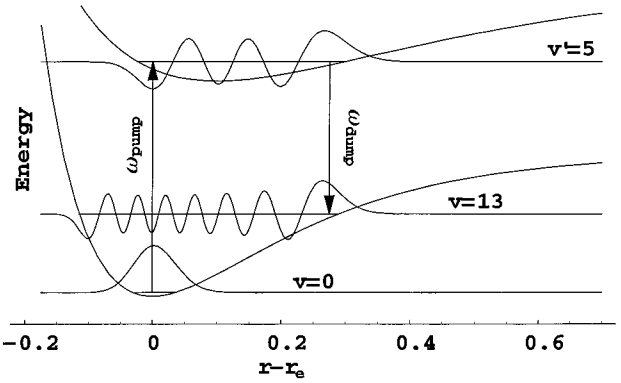

Figure 1. Stimulated emission pumping method as applied to NO. This figure shows the electronic energy as a function of the displacement of the atomic separation, r, from the equilibrium separation, r_e, for two electronic states of NO ($X^2\Pi$ and $B^2\Pi$). IN SEP molecules are excited out of ground state levels through an allowed transition to an excited electronic state with a distorted structure. Laser-induced emission transfers population back to single highly vibrationally excited quantum states of the ground electronic state. Three realistic vibrational wave functions are shown. Energies accessible with this method can be large (greater than 400 kJ/mol), and pumping can be efficient ($\sim 10^{-1-2}$).

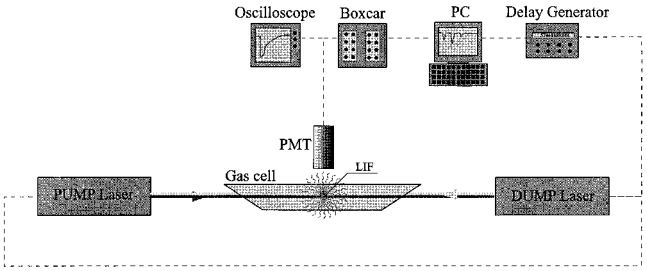

Figure 2. Experimental set up for detection of SEP transitions in a fluorescence dip experiment. PUMP laser induced fluorescence (LIF) is detected at right angles by a photomultiplier tube (PMT). Stimulated emission effected by the DUMP laser appears along the propagation axis of the DUMP laser and reduces the side fluorescence seen by the PMT. These "fluorescence dips" are recorded as a function of the DUMP laser frequency to map out the spectroscopy of highly vibrationally excited molecules. The signal indicated "on the oscilloscope" results when the DUMP laser is delayed with respect to the PUMP laser. By recording the early and late parts of the decay, the shot-to-shot fluctuations in the PUMP LIF can be accounted for and used to increase the *S*/*N* of the spectrum. Alternatively, two PMTs can be used, where one views the two laser signal and one views the PUMP LIF in a separate cell.

integral of the two vibrational states, $Q(v',v'') = |\int \chi_{v'}(r - r_e)\, \chi_{v''}(r - r_e)\, dr\}^2$, referred to as the Franck−Condon factor. Because of the large changes in the interatomic potential upon electronic excitation, the "Franck Condon matrix", $Q(v',v'')$, is highly nondiagonal favoring large changes in the vibrational quantum number for both the PUMP and DUMP steps. For the example shown in Figure 1, the strongest DUMP transitions result in very highly vibrationally excited states, e.g., $Q(v' = 5, v'' = 19) = 0.2$. The Franck−Condon principle explains why preparation of highly vibrationally excited molecules, in general, and NO in particular[27,28] is so straightforward.

The SEP transition may be detected in a number of ways including ion dips[29] and degenerate four-wave mixing.[30] However, due to its simplicity, the "florescence dip" method is used most commonly and has been a powerful tool for spectroscopic investigation of highly vibrationally excited molecules.[12,31] Figure 2 shows a schematic of this kind of experiment. The PUMP and DUMP beams are collinearly overlapped and a photomultiplier views the PUMP laser induced florescence

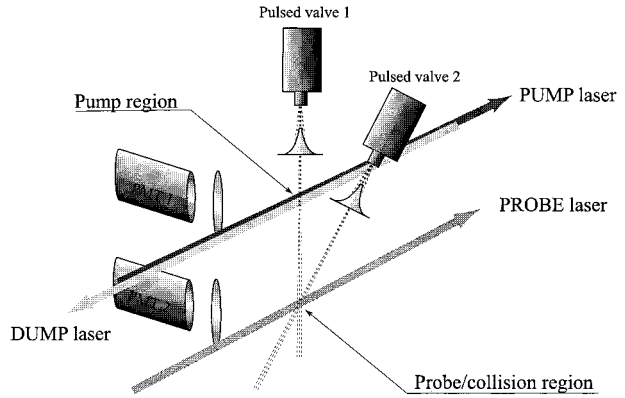

Figure 3. Crossed molecular beams with PUMP−DUMP−PROBE geometry. A molecular beam is excited by SEP preparing single quantum states of highly vibrationally excited molecules at the "pump region". PMT-1 views this region allowing fluorescence dip measurements. Several centimeters downstream, the sample is detected by the PROBE laser. When pulsed valve-2 is turned off, the results of infrared emission occurring during the flight time between preparation and detection can be observed (section 3.1). With pulsed valve-2 turned on, the results of single collisions are detected by the probe laser (section 3.2,3.3, and 3.5).

perpendicular to laser beams. When the DUMP laser hits stimulated emission resonances, spontaneous side florescence is reduced and stimulated emission along the DUMP laser propagation axis is increased. Shot-to-shot normalization to the fluctuating PUMP laser intensity, using either the dual-beam[32] or double-boxcar[33] approach, allows detection of dips as small as 1%.

We can also use a third laser to probe the sample after the preparation of the highly vibrationally excited molecules. We refer to this as the "PUMP−DUMP−PROBE" geometry. When done in a cell, state-to-state kinetics measurements are possible. Alternatively, one may use molecular beams (Figure 3). Here, the molecules prepared with SEP are detected by laser-induced fluorescence (LIF) at a different position and time. Likewise, resonant enhanced multiphoton ionization (REMPI) detection is possible. The temporal and spatial separation of the preparation step from the detection step allows detection of much weaker transitions and, of course, provides a probe of collisional events.

PUMP−DUMP−PROBE experiments make up most of what is described in this article. This approach has allowed SEP to go beyond spectroscopy of super-excited molecules and begin providing information on their collisional properties. Highlights of our research using PUMP−DUMP−PROBE are presented in section 3, progressing from the simple to the complex. In this spirit, we start with an example of *collision-free* relaxation (infrared emission). We then proceed sequentially to examples of rotational energy transfer, vibrational energy transfer, and energy transfer at solid surfaces. We then turn briefly to one of the first examples of vibrationally enhanced surface chemistry and finish by describing our serpentine exploration of atmospheric chemistry.

3. Highlights of Recent Work

3.1. Infrared Emission of Highly Vibrationally Excited NO. Radiation is perhaps the most common means of removing energy from an excited molecule. Emission and absorption of light can even be the dominant means of energy transfer, e.g., in interstellar space. Closer to home, one must only look to the night sky to witness super-excited molecules struggling toward nighttime equilibrium. An exothermic reaction, $H + O_3 \rightarrow O_2 + OH(v)$, produces OH radicals in states up to $v = 9$, resulting in intense emissions in the 1−3 μm region of the spectrum. These "Meinel atmospheric bands"[34,35] are one of the strongest atmospheric emissions of the night sky. Similarly, auroral emission in the 5 μm region[36] is attributed to NO($v \leq 9$), produced by nonthermal $N + O_2 \rightarrow O + NO(v)$.[37,38]

These examples show one of the curious properties of highly vibrationally excited molecules, infrared overtone emission. The two molecular properties that govern infrared emission (or for that matter absorption) are the dipole moment function, $\mu(r - r_e)$, and the intermolecular potential $V(r - r_e)$. Here r_e is the bond length at the minimum of the molecular potential. $V(r - r_e)$ governs the motion of the atoms and together with $\mu(r - r_e)$ dictates how the charge distribution oscillates in time.

For a diatomic molecule, if the dipole moment function is linearly proportional to $r - r_e$ and the intermolecular potential is harmonic, i.e., $V(r - r_e) \propto (r - r_e)^2$, only fundamental transitions ($\Delta v = \pm 1$) are possible. In general, for low vibrational states, the variation of $r - r_e$ is small. As a result, even an anharmonic $V(r - r_e)$ may be assumed harmonic and a nonlinear $\mu(r - r_e)$ may be assumed linear. Consequently, only $\Delta v = \pm 1$ transitions are in general observed for low vibrational states of most molecules.

However, for super-excited molecules, both the curvature of $\mu(r - r_e)$ (electrical anharmonicity) and the anharmonic nature of $V(r - r_e)$ (mechanical anharmonicity) are not negligible. This can mean that overtone emission becomes just as important as fundamental emission. To illustrate this, Figure 4 shows the wave functions for $v = 0$ and 25 of NO along with the true interaction potential and dipole moment function.[39] For comparison, we also show the harmonic approximation to the interaction potential and linear dipole moment function.

The interaction potential can be found from high precision spectroscopic constants, using the semiclassical Rydberg−Klein−Rees (RKR) approach.[40−42] Finding the dipole moment function requires accurate measurements of transition intensities and is, therefore, more difficult.[43−45] The experimental setup shown in Figure 3 allows a direct determination of the rates and branching ratio's for infrared emission from high vibrational states, yielding the dipole moment function over a wide range of vibrational amplitude.

Figure 5 shows two spectra of NO($v = 19$) and their difference (bottom panel). In both of these spectra, the PUMP laser excites ground-state NO to the $B^2\Pi$ state, preparing a single $J = 2.5$ level at the preparation zone (see Figure 3; only one molecular beam is used) and spectra are recorded 6 cm downstream at the detection zone. In the top panel, the detected states are populated by spontaneous visible emission out of the B state, the selection rules for which favor population of $J =$ 3.5 and 1.5. A barely detectable signal from $J = 4.5$ is also seen, apparently violating the $\Delta J = \pm 1$ selection rules. These levels are populated by two stages of emission: visible $B \rightarrow X$ emission to vibrational states above $v = 19$ (in $J = 1.5$ and 3.5) followed by infrared emission to $v = 19$ (populating $J =$ 0.5, 2.5, and 4.5).

Consider now the middle panel of Figure 5. Here, the DUMP laser stimulates emission to $|v = 21, J = 3.5\rangle$, two vibrational quanta above the probed state. With the DUMP laser on, some lines in the probe spectrum go up and some go down compared to the lines in the top panel. This is clearer from the difference spectrum (lower panel). Some lines (probing population in $J =$ 1.5 and 3.5) lose intensity as population that was bound for v $= 19$ is forced into $v = 21$ by stimulated emission. Other lines

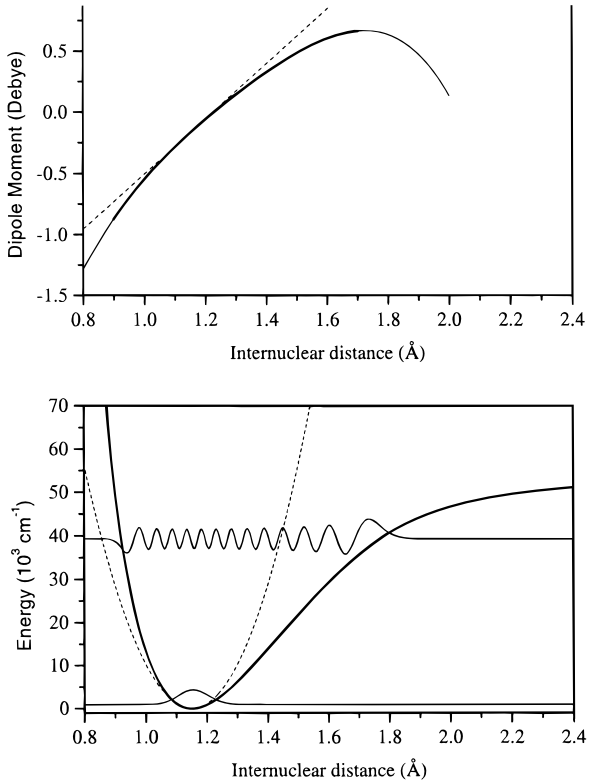

Figure 4. Vibrational wave functions and potential energy curve for NO($v = 0$ and 25) in its ground electronic state. The thick black line in the upper panel shows the dipole moment function for NO as determined in our experiments. The thin line is an extrapolation to shorter and longer bond distances. Clearly, the linear approximation, given by the dotted line, is only valid in a small interval around the equilibrium distance. The lower panel shows the NO potential determined by the RKR procedure, see text, and the corresponding wave functions for $v = 0$ and $v = 25$. The harmonic approximation of the potential, given by the dashed line, is only useful for the lowest vibrational levels.

(probing population in $|v = 19, J = 2.5$ and $4.5\rangle$) gain intensity, as the SEP prepared state $|v = 21, J = 3.5\rangle$ radiates to them.

Using the flight time between preparation and detection, we could derive the infrared emission rates, that is, the Einstein *A* coefficients.[39] By doubling the DUMP and PROBE laser light, the experiment was repeated on lower vibrational states. Combining these results with a conventional RKR analysis to determine the interaction potential, we were able to derive the dipole moment function between 0.9 and 1.7 Å (Figure 4) and predict all of the infrared emission and absorption properties of NO up to $v = 25$.[39]

This example shows some of the unusual properties of super-excited molecules. Even for isolated diatomics, our notions of simple molecular quantum mechanics are inadequate. We should not be surprised that more complex chemical events than emission and absorption of light are likewise replete with rich dynamics. The following sections present examples of what can happen when highly vibrationally excited molecules collide with other molecules.

3.2. Rotational Energy Transfer. Under most conditions, rotational energy transfer is the most likely outcome of any collision. How rotational energy transfer may differ for vibrationally excited state is, therefore, of significant interest. Our work has shown that, at least for diatomics, super-excited molecules behave like stretched ground-state molecules, the major influence of vibration being the lengthening of the average internuclear separation.

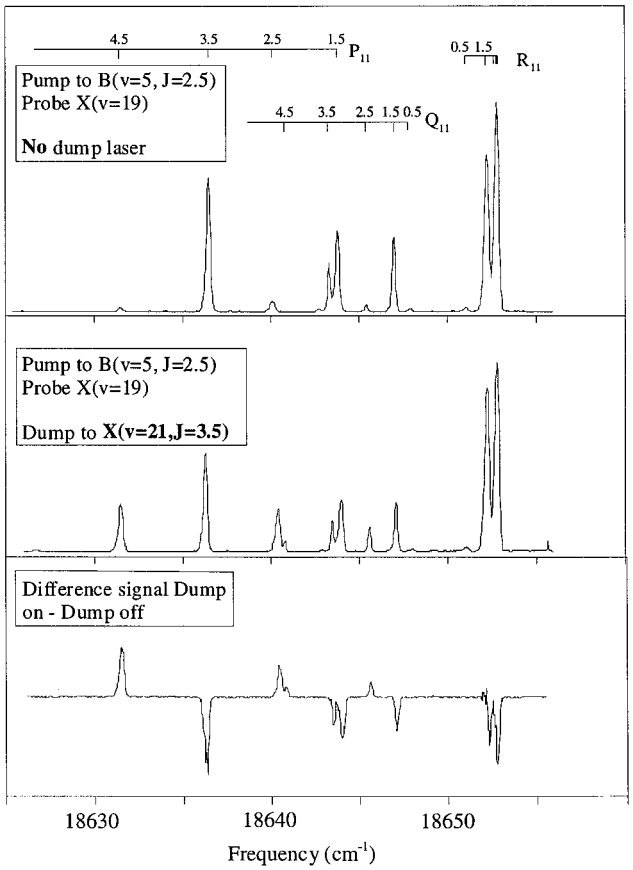

Figure 5. Infrared emission from highly vibrationally excited NO. When NO is excited with the PUMP laser preparing $B^2\Pi$ ($v = 5$, $J = 2.5$), spontaneous emission populates a whole host of vibrationally excited levels in the ground, $X^2\Pi$, electronic state. In the upper panel, we show an LIF spectrum of molecules in $X^2\Pi$ ($v = 19$) populated in this way. Due to the optical selection rules only $J = 1.5$, 2.5, and 3.5 should be present. In the middle panel, the same spectral region is scanned while the DUMP laser is stimulating a large fraction of the molecules from the $B^2\Pi$ ($v = 5$, $J = 2.5$) level to $X^2\Pi$ ($v = 21$, $J = 3.5$). Population observed in $J = 4.5$ and 2.5 increases due to infrared emission from $v = 21$ to $v = 19$, which is governed by $\Delta J = \pm 1$ selection rules. Population in $J = 3.5$ and 1.5 decreases due to the DUMP laser induced depletion of population in $B^2\Pi$ ($v = 5$, $J = 2.5$). The bottom panel shows the difference of the two spectra for clarity.

Early experiments on rotational energy transfer in cells revealed no unusual behavior for highly vibrationally excited molecules compared to vibrational ground state molecules.[46] More recently, we performed crossed molecular beams experiments on NO($v = 20$) colliding with He[47] to obtain more detailed information. The experimental arrangement is shown in Figure 3 (this time using two beams). For the crossed beams experiments, the collision energy is well defined since the beams possess narrow velocity distributions ($\Delta v/v \approx 0.1$) and are constrained to cross at a well-defined angle. In this experiment, the collision energy was 2.3 ± 0.8 kJ/mol, close to the average collision energy at room temperature. The use of molecular beams furthermore ensures that we observe single collision dynamics. The state preparation was also improved from the earlier experiments by the use of a high-resolution PUMP laser (Figure 6). This made it possible to specify all of the molecular quantum numbers ($|\Lambda, \Sigma, \Omega, v, J, e/f$ parity$>$ but not magnetic hyperfine sublevels) in addition to the translational energy of the collision.

Furthermore, the system is simple enough that high-level ab initio theoretical simulations of the experiment could be carried out. For comparison, quantum dynamical calculations carried

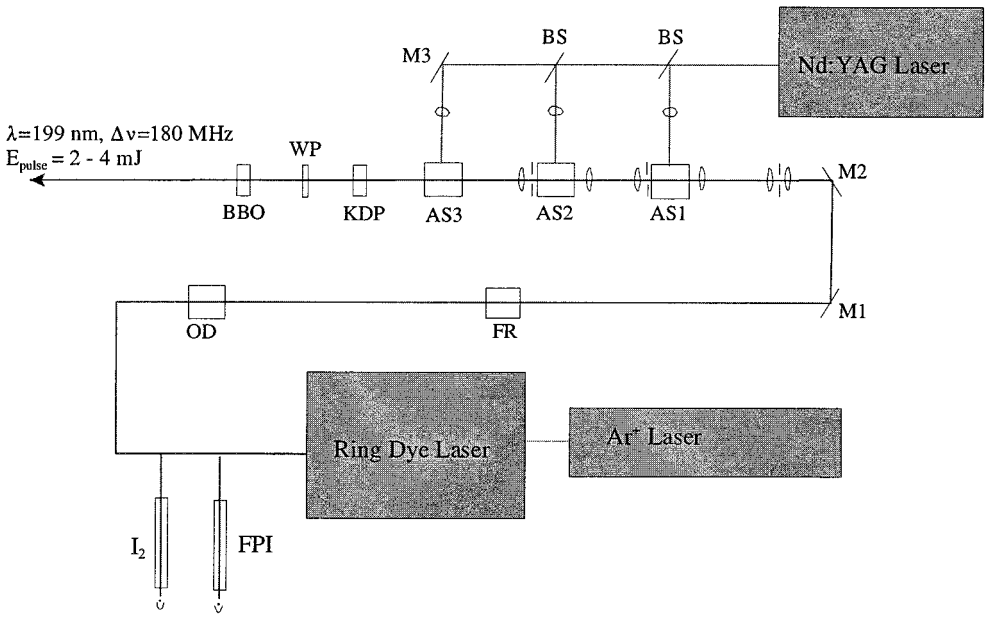

Figure 6. Schematic diagram of the pulsed dye amplifier system used in the molecular beam experiments. The output of an Ar ion laser pumped a ring-dye laser which is pulse-amplified in three stages (AS1−3) by the output of a Nd:YAG laser. After frequency-doubling the amplified light in a KDP crystal and subsequently mixing it with the fundamental light in a BBO crystal, radiation at a wavelength around 199 nm is generated with a bandwidth of 180 MHz and a pulse energy of 2−4 mJ. Frequency calibration is performed by recording the I_2 absorption spectrum and the transmission fringes of an Fabry−Perot interferometer (FPI). Legend: OD, optical diode; FR, Fresnel rhomb; M1−3, steering mirror; BS, beam splitter; WP, $\lambda/2$ wave plate.

out by Millard Alexander and co-workers were done on two potential energy surfaces.[47] The first surface was calculated fixing the bond length at $<r - r_e>$ of NO($v = 0$). The second surface fixed the NO bond length at the average bond length of NO($v = 20$).

Figure 7 shows the comparison of relative spin−orbit conserving collision cross sections, both measured and calculated for scattering of NO($v = 20$) from He. A marked oscillation in the scattering cross section is easily seen. For collisions that do not change the *e/f* parity, a ΔJ-even propensity is seen. For *e/f* parity changing collisions, one finds a ΔJ-odd propensity. This shows that the overall rovibronic parity is approximately conserved. While this result is visually striking, experiments on NO($v = 0$) show the same behavior.[48]

Careful inspection of Figure 7 shows that the calculations using the two potential surfaces give slightly different but experimentally distinguishable results. This arises from the fact that the "stretched NO potential" exhibits a larger degree of angular anisotropy, resulting in somewhat larger values of ΔJ more closely matching experiment. This work gives a simple picture for rotational energy transfer of highly vibrationally excited diatomics. Despite the large-amplitude vibrational motion in $v = 20$, the time scale separation of rotation and vibration simplifies the dynamics. The angular forces exerted on the diatomic by the collision are averaged over the vibrational motion, making a stretched rigid rotor model suitable. Well-controlled experiments and comparison to high-quality theory are required to observe the subtle differences in rotational energy transfer exhibited by super-excited molecules. Observing the unusual vibrational relaxation properties of these species is a much simpler matter.

3.3. Vibrational Energy Transfer. In general, vibrational energy is converted to translation and rotation (V−R,T) of the scattered molecules or to vibration (V−V) of the collision partner. Super-excited molecules possess so much vibrational energy that excited electronic states (V−E) also come into consideration. Highly vibrationally excited molecules may approach transition states of chemical reactions, even very endothermic ones. For collisions that approach the transition state but fail to react, the forces exerted on the vibrationally excited bond may induce efficient vibrational energy transfer.[49]

Our first foray into this problem involved SEP experiments preparing highly vibrationally excited NO in a cell.[46,50] We measured total removal rate constants for NO self-relaxation over a wide range of vibrational states with energies between 160 and 450 kJ/mol. This gave the first look at the vibrational quantum number dependence of vibrational deactivation over such a wide energy range. A threshold for enhanced vibrational relaxation appeared at about $v = 13$. Below $v = 13$, the relaxation rate constant was proportional to vk_1, where k_1 is the $v = 1$ relaxation rate constant. Linear dependence on v is a prediction of SSH theory[51] of V−R,T energy transfer, resulting from making the interaction potential linear and using harmonic oscillator wave functions. Above $v = 13$, relaxation rates increased much faster than linearly so that NO in $v = 24$ relaxed more than 200 times faster than in $v = 1$.

It is interesting to note that NO($v = 13$) lies close in energy to the theoretically predicted activation barrier for formation of the lowest of a series of high-energy isomers of the NO dimer.[52] Furthermore, the calculated structure at the barrier is asymmetric, with one short (1.184 Å) and one long (1.439 Å) NO bond. The short NO bond resembles ground-state NO. The lengthened NO bond is somewhat shorter than the most probable bond length of NO in $v = 13$ ($r_{mp} = 1.52$ Å). We speculate that collisions between one vibrationally excited NO molecule and one in $v = 0$ could access this isomer. Complex formation would explain more efficient vibrational relaxation above $v = 13$. We might also expect multiquantum ($\Delta v \leq 1$) relaxation to take place. Experiments carried out on $v = 19$ indeed confirmed the importance of multiquantum relaxation. In light of these results, it is interesting (and logical) to speculate that complex formation is responsible for the enhanced vibrational deactivation of NO above $v = 13$, but the truth behind this conjecture awaits future study.

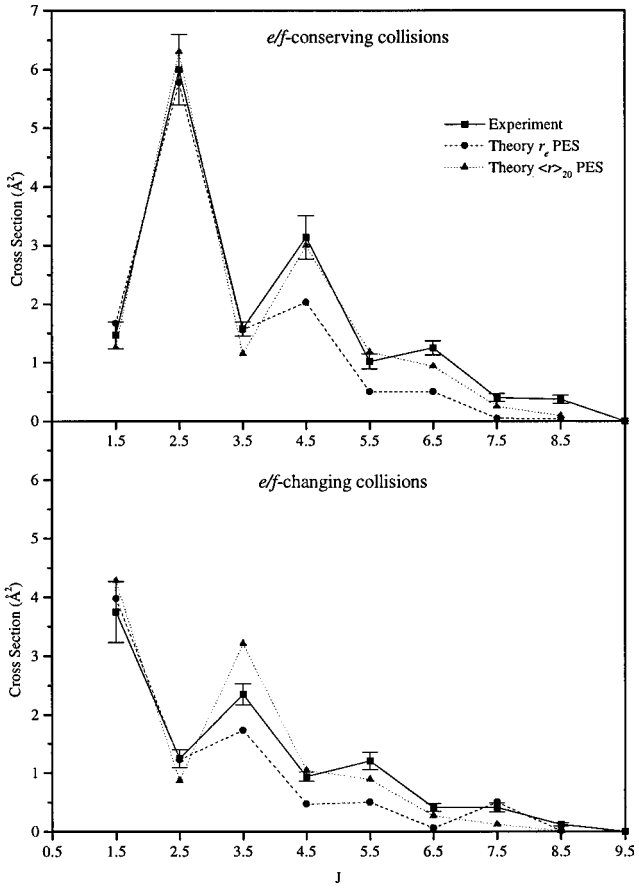

Figure 7. Comparison of the experimental and theoretical cross sections for spin−orbit conserving ($\Omega = {}^1/_2 \rightarrow \Omega = {}^1/_2$) collisions between NO($v = 20$) and He. Upper panel: *e*/*f*-conserving transitions. Lower panel: *e*/*f*-changing transitions. The circles with error bars are the experimental points. The circles without error bars are the theoretical values using a potential energy surface where the NO bond length is fixed at the average value of $v = 0$. The triangles are theoretical values from a second potential energy surface where the NO bond length is fixed at the average value of $v = 20$. The agreement shows that the rigid rotor pituce of rotational energy transfer for NO($v = 20$) is still a good one.

Let us now consider the nature of a near resonant vibrational−vibrational (V−V) energy transfer for super-excited molecules. If a diatomic molecule formed in a high vibrational state relaxes one vibrational quantum at a time, due to anharmonicity the amount of energy transferred slowly increases as the relaxation progresses. For near resonant V−V energy transfer, the relaxing super-excited molecule effectively scans a range of frequencies in the acceptor molecule. The range of "scanned" acceptor frequencies can be quite large. Look, for example, at O_2. If 1−1 and 2−1 resonances are considered,

$$O_2(v) + A(0) \rightarrow O_2(v - 1) + A(1)$$

$$O_2(v) + A(0) \rightarrow O_2(v - 2) + A(1)$$

an O_2 molecule relaxing from $v = 27$ down to $v = 0$ scans a range of acceptor molecule frequencies from ~1000 ($v = 27 \rightarrow 26$) to 3200 ($v = 2 \rightarrow 0$) cm^{-1}. Clearly, such a molecule experiences manifold opportunities to exchange quanta of vibration with its environment.

We have become interested in highly vibrationally excited O_2 because of its possible significance to stratospheric ozone formation (see section 3.5). This led us to carry out painstaking measurements of the vibrational relaxation rate constants,

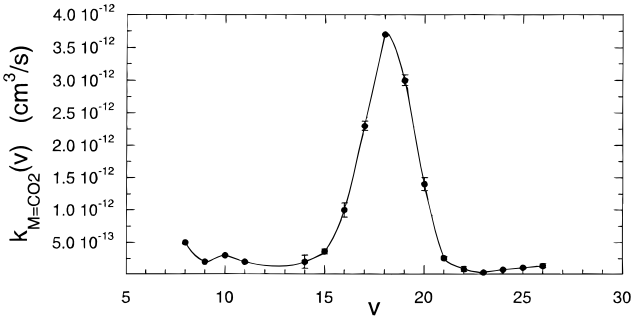

Figure 8. 2−1 resonance in vibrational relaxation of $O_2(v)$ by CO_2. The sharp resonance at $v = 18$ indicates the dominant relaxation channel: $O_2(v) + CO_2(000) \rightarrow O_2(v - 2) + CO_2(001)$. Such 2−1 resonances are commonly seen for highly vibrationally excited molecules and exhibit cross sections as large as the better-known 1−1 resonances. The $v = 8-11$ points were taken from the following work: Klatt, M.; Smith, I. W. M.; Symonds, A. C.; Tuckett, R. P.; Ward, G. N. *J. Chem. Soc., Faraday. Trans.* **1996**, *92*, 193.

hereafter referred to as $k_M^{O_2}$ of $O_2(v)$ with a number of typical atmospheric collision partners. These included M = O_2, O_3, N_2, CO_2, and N_2O. In every case, we have found strong evidence for near resonant V−V energy transfer.[53,54]

An illustrative example of V−V transfer is shown in Figure 8, where the vibrational relaxation rate constant for the CO_2−O_2 system, $k_{M=CO_2}^{O_2}(v)$, is plotted as a function of O_2 vibration. The vibrational relaxation is dramatically enhanced (by about a factor of 100) near $O_2(v = 18)$. The 2−1 near-resonant energy transfer process responsible,

$$O_2(v) + CO_2(000) \rightarrow O_2(v - 2) + CO_2(001)$$

has a minimum energy defect of only a few wavenumbers for $O_2(v = 18)$. More direct evidence for the 2−1 resonance came from PUMP−DUMP−PROBE experiments preparing $O_2(v = 17)$ in mixtures with CO_2 and watching the population evolve in $v = 16$ and 15. In these experiments, one can see that population initially in $v = 17$ skips $v = 16$ and appears in $v = 15$. Similar 2−1 and 1−1 resonances were found to be important for all the systems studied.

Since near-resonant V−V transfer appears to be so common, we wish to understand its nature better. From a perturbation-theoretical point of view, minimizing the energy defect enhances the transfer probability. However, we do not know which molecular motions effectively compensate for the inevitable finite energy defect. What allows energy defect compensation is the essential physical element determining the resonance widths and thereby the overall importance of V−V transfer.

For small defects (~20 cm^{-1}) optical-like selection rules explain V−V energy transfer well.[55,56] This implicates the importance of long-range, high impact parameter interactions (e.g., dipole−dipole or dipole−quadrupole) and requires ΔJ to be small, even in higher orders of perturbation theory. By necessity, this approach means that rotational motion does not effectively compensate the energy mismatch. These models, however, underestimate the importance of V−V energy transfer for larger energy defects.[57] This suggests that rotational motion may be important, a suspicion further supported by measurements of the temperature dependence of V−V transition probability.[58]

The role of rotation in compensating for the energy defect is also supported by the observation that, in vibrationally elastic energy transfer, many rotational quanta can be exchanged. Determining the relative importance of rotation vs translation in compensating for the energy defect has, however, remained

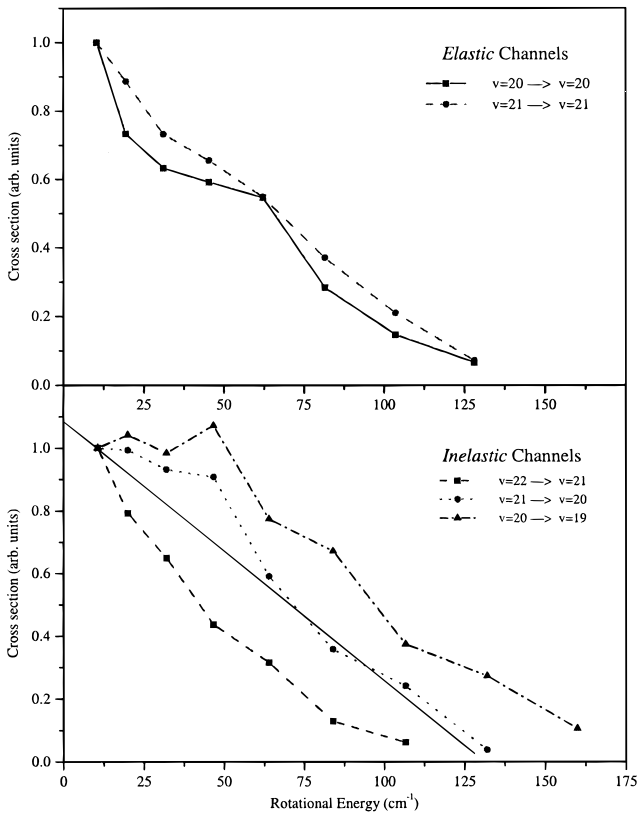

Figure 9. Rotational compensation of the energy defect in V−V energy transfer. In the upper panel, we show relative vibrationally elastic state-to-state cross sections for NO $X^2\Pi$ ($v = 20$ and 21, $J = 0.5$) collisions with N_2O (collision energy 125 cm^{-1}). In the lower panel, we compare state-to-state cross sections for vibrational inelastic channels to those for the vibrationally elastic channel (Solid line). As the prepared vibrational state is varied, so is the energy deficit for the near resonant V−V transfer. The rotational distribution of the scattered NO clearly shifts to compensate the change in energy deficit. (See section 3.5)

a difficult problem in the field of molecular energy transfer, and little direct experimental evidence is available.

The PUMP−DUMP−PROBE technique in combination with molecular beams allows us to gain insight into this intriguing question. We studied the specific example

$$NO(X^2\Pi,v) + N_2O(0,0,0) \rightarrow NO(X^2\Pi,v-1) + N_2O(0,0,1)$$

using the setup shown in Figure 3.[59] Here, (v_1,v_2,v_3) indicates the number of quanta excited in the symmetric-stretch, bend, and asymmetric-stretch, respectively.[60] Vibrational relaxation was observable for NO($v = 20$, 21, and 22), where the energy defect is −49, −18, and +14 cm^{-1}, respectively. Energy transfer was found to be approximately 5 times more efficient for the $v = 21$ level than for the other two vibrational levels. For $v = 19$ and 23, which have energy defects of −80 and +47 cm^{-1}, respectively, no vibrational energy transfer could be detected.

Energy transfer from $v = 22 \rightarrow 21$ ($\Delta E = +14$ cm^{-1}) was found to be substantially less efficient than that from $v = 21 \rightarrow 20$ ($\Delta E = -18$ cm^{-1}), despite the availability of 125 cm^{-1} of kinetic energy. This is direct evidence that translational energy is not effective in compensating for the positive energy defect. The role that rotations play in compensating for the V−V energy mismatch becomes clear when comparing the rotational energy distributions for vibrationally *elastic* and *ineleastic* channels. These are shown in Figure 9. The upper panel shows the relative state-to-state cross sections for vibrationally *elastic* transfer of NO($v = 20$ and 21, $J = 0.5$) with N_2O. The rotational energy transfer is quite similar for both vibrational levels in line with the results of section 3.2.[47]

In comparison, the lower panel of Figure 9 shows the (peak-normalized) relative state-to-state cross sections for the vibrationally *inelastic* channels. The rotational distributions are clearly shifted with respect to the vibrationally *elastic* distribution, given by the solid line. The endoergic channel ($v = 22 \rightarrow 21$) is rotationally cooled, whereas the two exoergic channels are rotationally hotter. The observed shifts in the rotational distributions correspond almost exactly to the V−V energy mismatch for these channels. This clearly shows that the energy defect, which is varied smoothly in the experiment, is nearly completely compensated for by NO rotational energy.

These results indicate that rotational motion is effective in compensating for the energy mismatch in near-resonant V−V transfer. In light of this, it is clear that the overall importance of V−V energy transfer can be dramatically underestimated if the role of rotational excitation is not adequately accounted for.

3.4. Super-Excited Molecules Colliding With Surfaces. Up to this point, we have only considered gas-phase collisions of super-excited molecules. When a vibrationally excited molecule in the gas-phase collides with a *solid*, energy can be transferred to electronic states and phonons of the solid, in addition to the conversion of vibrational energy to rotational and translational (V→R,T) energies. The large number of energy-accepting degrees of freedom in the solid can lead to different energy transfer dynamics and can dramatically influence the rate of energy transfer. For molecules in low-lying vibrational states, several mechanisms for vibrational energy transfer have been identified. These include excitation and de-excitation via trapping (long-lived complexes),[61,62] nonadiabatic (i.e., vibrational-to-electronic) coupling,[63] direct "mechanical coupling",[64] and stretching of bonds in frustrated surface chemical reactions.[65,66]

Which of these or other dynamics are important for vibrational energy transfer involving super-excited molecules at surfaces? How will the probability of vibrational energy transfer change for highly excited molecules? Will vibrational relaxation rates scale with the vibrational energy of the initial state as theory predicts?[67,68] At present, we have almost no direct experimental data to address these important questions.

Figure 10 shows an experimental apparatus, recently developed in our laboratory, that is providing some of the first information on how highly vibrationally excited molecules interact at solid interfaces. A pulsed molecular beam is excited by the PUMP and DUMP lasers. A photomultiplier views the region where the laser beams cross the molecular beam allowing fluorescence dip measurements to characterize the optical excitation efficiency. The highly vibrationally excited NO molecules then travel through a set of differential pumping apertures and enter the ultrahigh vacuum (UHV) scattering chamber where they collide with a crystalline copper (111) surface at normal incidence. The scattered NO molecules are ionized with REMPI, and the ions are extracted back along the original direction of the molecular beam and turned 90° off-axis to a two-stage multichannel plate detector.

As copper is slowly oxidized by exposure to NO,[69−71] experiments were carried out on the O-covered copper surface. Oxygen adlayers on copper were prepared by exposure of the clean Cu(111) surface to NO_2 followed by elevating the surface temperature to 800 K for several seconds. This ensured that only chemisorbed O atoms remain on the surface. After calibrating the Auger electron spectrometer's (AES) response against a previous study,[71] the ratio of AES signals for Cu and

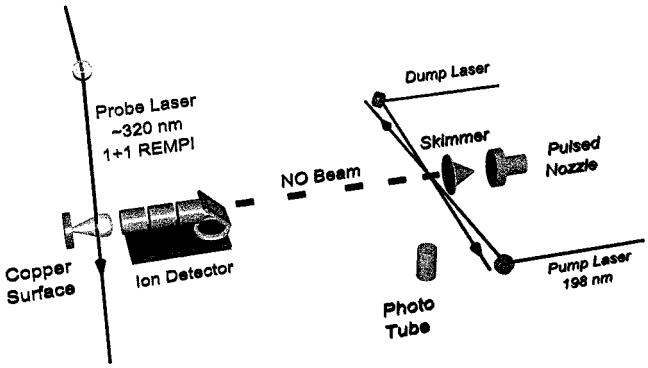

Figure 10. Experimental apparatus for studying the interactions of highly vibrationally excited molecules with solid surfaces. PUMP and DUMP lasers prepare highly vibrationally excited NO in the second differential pumping chamber downstream from a pulsed molecular beam of NO. A photomultiplier tube is used for fluorescence dip spectroscopy, which helps control the optical excitation step. PUMP laser induced fluorescence was also monitored by a photomultiplier for signal normalization. The excited molecules travel through one more region of differential pumping and collide with a well-characterized copper surface or oxygen adlayer on copper. Scattered NO is state selectively ionized using 1+1 REMPI. The ions are extracted back along the molecular beam direction and deflected by a 45° plate to a microchannel plate detector. By scanning the frequency of the probe laser, we could measure the vibrational and rotational state distribution of the scattered NO. Translational energy distributions of the products are measured by recording the intensity of the REMPI signal as a function of the time delay between the excitation and the probe lasers. Angular distributions were recorded by translating the probe laser across the direction of incident molecular beam.

O on this surface revealed a ratio of O adatom to surface Cu atom of ~1:3.

Experiments carried out with this apparatus showed the most remarkable and efficient vibrational energy transfer process we have ever seen, where up to five quanta of NO vibration are transferred to an O atom covered copper surface.[72] Figure 11 shows a portion of the REMPI spectrum obtained when NO, with a mean kinetic energy of 63 kJ/mol and initial state $|v = 15, J = 2.5, \Omega = 0.5\rangle$ is incident on the O/Cu(111) surface and the scattered NO is detected with the probe laser tuned in the vicinity of the A(4) ← X(13) γ-band. The solid lines in the figure are the results of a least-squares fit to the data using an experimentally determined laser line shape function and theoretical (nonadjustable) transition frequencies and line-strengths. The upper panel in Figure 11 shows results of a fit that included both the A(4) ← X(13) and the A(2) ← X(10) γ-bands. The excellent agreement with the data shown is typical of the entire spectrum over some 500 cm^{-1}. The lower panel in the figure shows the resulting fit if only the A(4) ← X(13) γ-band is simulated. Clearly, the fit is inadequate. Figure 11 gives unambiguous evidence that both $\Delta v = -2$ and -5 vibrational relaxation channels are important for the scattering of NO($v = 15$).

Figure 12 shows the relative probabilities for the observed vibrational relaxation channels. Due to technical problems, it was not possible to record reliable data for channels transferring more than five quanta of vibration, but there is every reason to believe that, with experimental improvements, they will also be observed.

We also observe that the rotational distribution of the scattered molecules (that can be well described by a temperature) far exceeds the surface temperature. Furthermore, the rotational temperatures depend on the initial translational energy of the molecular beam. These results certainly indicate that trapping

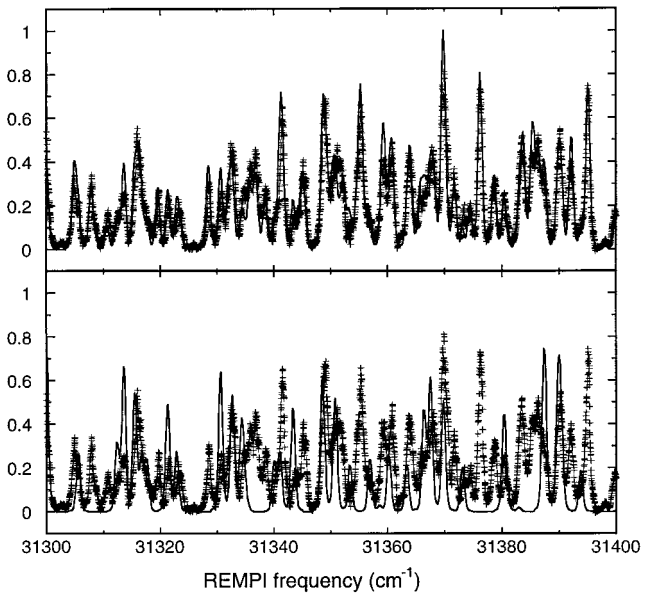

Figure 11. Scattering of NO($v = 15$, $J = 2.5$, $|\Omega| = 0.5$) from an O-covered copper surface. The REMPI spectrum (+) of the scattered molecules is shown compared to two modeled fits (solid lines). Upper panel: fit includes contributions from both the A(4)−X(13) and A(2)−X(10) γ bands. Lower panel: fit includes contributions from only the A(4)−X(13) γ band. This shows clearly that NO($v = 15$) scatters from the surface in $v = 13$ and 10. Other spectra also showed $\Delta v = 0$, -1, -3, and -4.

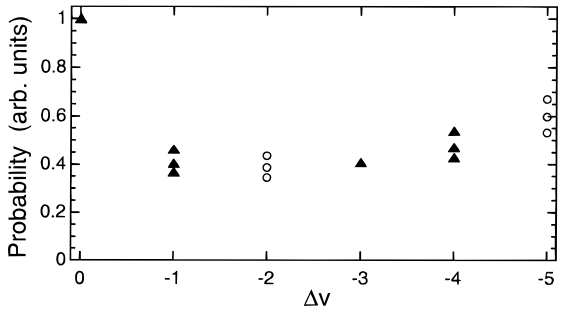

Figure 12. Multiquantum relaxation: scattering probabilities. Probability of scattering as a function of change in vibrational quantum number. All data correspond to a kinetic energy of 29 kJ/mol. Values were obtained from experiments with incident NO($v = 15$) (○) and incident NO($v = 13$) (▲). The three sets of points correspond to three alternative interpretations of the raw data. See Hou et al.[75]

followed by desorption from the surface is not responsible for the observed multiquantum relaxation. We also see that rotational energy in the scattered molecules accounts for less than 7% of the available energy and the average translational energy of the scattered molecules is nearly equal to that of the incoming beam. One should note that the velocity resolution of our present experiment needs to be improved. Small changes in velocity upon impact are not yet ruled out. The very small changes in rotational and translational energy with Δv indicate that the rotation and translation are effectively "spectator" degrees of freedom during the collision and that vibrational energy is transferred to surface degrees of freedom.

Observations such as this have no precedent in the study of molecular energy transfer, and two mechanisms that could explain them are under investigation. The electron affinity of NO depends strongly on the internuclear distance, increasing from near zero at r_e to about 3 eV at the outer classical turning point of $v = 15$. For this analysis, approximate Lennard-Jones potentials for NO and NO^- give the electron affinity as a function of internuclear separation. This suggests an electron

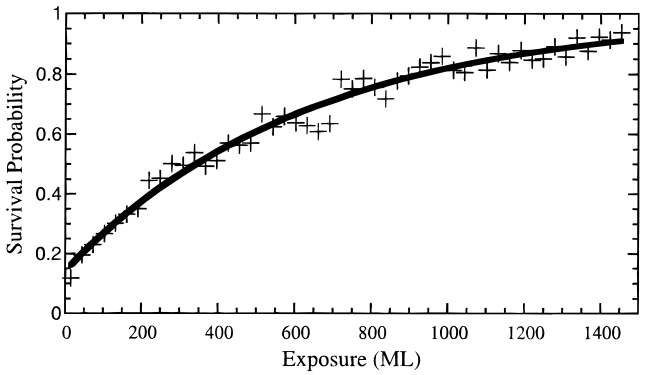

Figure 13. Reaction of NO($v = 13$) on copper. Survival probability of NO($v = 13$) as a function of surface exposure to the oxidizing action of ground state NO. The growth in the survival probability is explained by decreased reactivity of highly vibrationally excited NO on the O-covered copper surface. The reaction probability is close to unity. Compare this with the reaction probability of ground-state NO (0.0002).

might jump from the metal to an NO($v = 15$) molecule during a collision with the surface. At some point later, the electron could jump back to the surface. Transient negative ion formation would impart a large force to the NO bond, since the NO and NO^- interaction potentials are very different. Furthermore, it would provide a mechanism where vibration is directly coupled to the surface and not to rotation and translation.

Preliminary calculations using a model to describe transient negative ion formation have shown some success; however, further experiments are required to rule out other possibilities. For example, NO_2 is bound to copper at low temperature. Therefore, super-excited NO might transiently form a highly excited NO_2* adsorbate in collisions with an O-covered copper surface. If the lifetime of adsorbed NO_2* were short (subpicosecond), it might decompose back to gas-phase NO and the scattered molecules might exhibit the behavior seen in this work. Clearly, there is much to do before these issues can be clarified.

In light of the observations of the last section showing that vibrational relaxation at solid surfaces can be remarkably efficient, one wonders how effective vibrational energy can be in driving surface reactions. Previous studies of this issue were restricted to low-lying vibrational states, populated either thermally[73] or with optical excitation.[74] The reaction probabilities observed, although strongly influenced by vibration, were low (10^{-2}). Can it be that vibrationally enhanced reaction probabilities greater than this will be generally frustrated by the remarkable vibrational quenching possible at surfaces?

In the last section, we mentioned that copper is slowly oxidized by ground state NO. Consequently, we looked at vibrational relaxation on an O-covered copper surface. Figure 13 shows the time dependence of the REMPI signal resulting from vibrationally elastic scattering of NO($v = 13$) during the oxidation of copper by ground-state NO.[75] The solid line is a fit based on first-order kinetics. This shows the survival of specific states of highly vibrationally excited NO decreases when the oxygen adlayer is absent from the surface.

There are two possible explanations for this observation. First, vibrationally inelastic channels could be more probable on the clean copper surface in comparison to the oxidized surface. In this case, the "missing $v = 13$ signal" at low exposures, should appear as enhanced signal for other vibrational states. That is, we expect to observe a *decrease* in signal with exposure for lower energy vibrational states that are populated by the supposed enhanced vibrationally inelastic energy transfer on clean copper. The second explanation is that the highly vibrationally excited NO reacts by adsorbing onto the clean copper surface, but cannot react on the oxidized surface. In this case, we expect to see a growth in all of the inelastic channels with exposure as the surface is transformed from its reactive form (copper) to its inert form (oxidized copper).

We failed to find any inelastic channels that exhibited different dependence to surface NO exposure than that shown in Figure 13, despite being able to sensitively detect inelastic channels up to $\Delta v = -5$. In fact, for a fixed surface temperature, all of the growth curves were quantitatively identical, suggesting they reflect the same kinetic process. This is compelling evidence that highly vibrationally excited NO reacts on a clean copper surface. Presumably, oxidation of the copper surface by ground state NO removes the sites where reaction can take place. Consequently, under surface oxidized conditions, inelastic channels dominate.

Using data like that shown in Figure 13, we find that the reaction probability for NO($v = 13$ and 15) on Cu(111) is close to unity. This can be compared to the reaction probability for ground-state NO on clean copper ($P_{v=0} = 0.0002$), which can be extracted from kinetic data like that shown in Figure 13. The vibrational promotion of this reaction is more than a factor of 5000.

We are just starting to learn about the influence of reactant vibration on surface reactivity, but it is already clear that the remarkable vibrational relaxation observed on O-covered copper does not rule out efficient vibrational promotion of surface chemistry.

3.5. Highly Vibrationally Excited O_2 in the Stratosphere. Our interest in super-excited molecules sprang from a desire to improve our fundamental understanding of the microscopic world of molecular interactions and dynamics. However, during the course of our studies, we have come to see that highly vibrationally excited molecules may be involved in stratospheric ozone formation. This realization pulled us headlong into the fascinating world of atmospheric chemistry, a field where fundamental molecular interactions can influence problems of interest to everyone.

The high UV flux characteristic of the upper atmosphere enhances photochemical reaction rates, which can accelerate the production of highly energetic molecules. Because the pressure is low (e.g., a few Torr at 40 km), collisional relaxation is slow. These two conditions can conspire to drive the internal energy distribution of atmospheric constituents far from equilibrium.

Photodissociation of ozone,

$$O_3 + h\nu \rightarrow O + O_2$$

is a typical example of this. The bond dissociation energy, $D(O_2{-}O) = 101$ kJ/mol, is low, and the absorption spectrum stretches from the visible to the deep ultraviolet, corresponding to photon energies from 200 to 600 kJ/mol. Consequently, the energy available to the photochemical reaction products, E_{ava}, is large. For example, at 226 nm, where some of our experiments have been carried out,[76] the products must dispose of 428 kJ/mol of excess photochemical energy.

At this wavelength, the majority of dissociation events result in electronically excited products,

$$O_3 + h\nu \rightarrow O(^1D) + O_2(a^1\Delta)$$

referred to as the singlet channel. About 10−15% of the time, ground electronic state products are produced

$$O_3 + h\nu \rightarrow O(^3P) + O_2(\chi^3\,E_g^-)$$

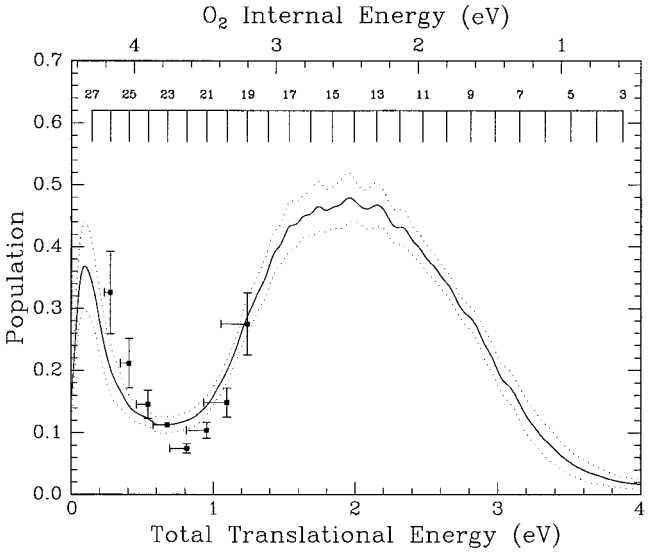

Figure 14. The product energy distribution in ozone photolysis at 226 nm. The translational energy distribution (solid line, bottom *x*-axis) is compared to the vibrational distribution (solid points, upper *x* axis). This shows that O_2 vibrational states are produced up to the energetic limit; see text.

In this so-called triplet channel, the available energy can only appear as relative translation of the products, E_{trans}, or internal energy (rotation, $E^{O_2}_{rotation}$ and vibration, $E^{O_2}_{vibration}$) of $O_2(\chi^3 E_g^-)$. Conservation of energy dictates that the internal energy of O_2 and translational energy are balanced.

$$E_{ava} = E_{trans} + E^{O_2}_{rotation} + E^{O_2}_{vibration}$$

This means that measuring E_{trans} gives the internal energy of the O_2 photoproduct.

The solid line in Figure 14 shows the relative translational energy distribution of the triplet channel of ozone photolysis at 226 nm[76] obtained in Paul Houston's lab using the ion imaging method.[77] The lower *x*-axis indicates total translational energy, and the upper *x*-axis shows the corresponding internal energy of the O_2 product.

The partitioning of the internal energy between rotational, vibrational, or electronic excitation can be found using laser-induced fluorescence (LIF). We photolyzed ozone under similar conditions to the Houston experiment, using LIF to probe the $O_2\chi^3 E_g^-$ products.[76] The state-specific LIF intensities gave information about the shape of the vibrational state distribution of the nascent products. These points are shown in Figure 14. The shape of the vibrational distribution is consistent with the translational energy distribution only if the internal energy of the O_2 is mainly vibrational. These two experiments give the unexpected result that stratospheric photodissociation of O_3 can produce vibrationally excited states of up to the energetic limit.

As described in section 3.3, we have used the PUMP−DUMP−PROBE method to examine the collisional behavior of highly vibrationally excited O_2. Figure 15 shows the self-relaxation rate constants, $k^{O_2}_{M=CO_2}(v)$ for highly vibrationally excited O_2. We also show the rate constants calculated from first-principles theory,[78] which agree remarkably well below $v = 25$. The slow decline in rate constant with v between $v = 8$ and ~20 reflects 1−1 resonant V−V energy transfer, which is important at low v but is overtaken by V−R,T energy transfer at high v. More interestingly, the rate constants for collisional removal of vibrationally state selected $O_2\chi^3 E_g^-$ exhibit a distinct threshold above $v = 25$.[53,54,79,80] Above this threshold

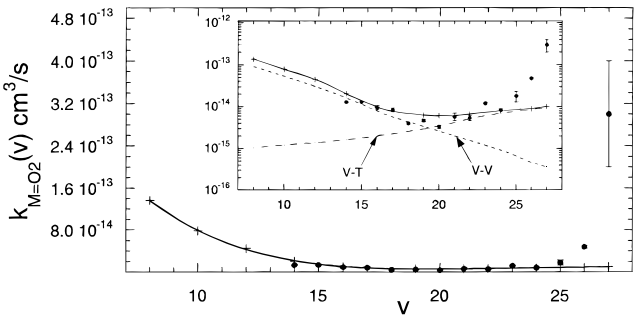

Figure 15. Vibrational self-relaxation of $O_2(v)$. Experimental rate constants for vibrational relaxation of specific vibrational states of O_2 in collisions with O_2 (●) are compared to theoretically calculated values (+) from (Hernandez-Lamoneda et al., 1995). Theoretical contributions from V−V and V−T mechanisms are shown in the insert. These calculations were carried out on an ab initio potential energy surface The excellent agreement below $v = 25$ shows the outstanding quality of the theoretical treatment. Above $v = 25$, a new relaxation channel clearly opens which is not accounted for by this treatment. The potential energy surface used in this work did not allow for reaction, $O_2 + O_2 \rightarrow O + O_3$, or energy transfer to excited electronic states of O_2, two possible explanations of the rapid increase in relaxation above $v = 25$. The same results with a logarithmic *y*-axis are shown in the inset.

removal rate constants rise steeply, indicating a change in the mechanism of collisional removal, and are no longer in agreement with theory.

Finding out what is responsible for the large acceleration in the relaxation rates above $v = 25$ has been one of the major goals of our research over the past few years. The energetic threshold for the reaction, $O_2 + O_2 \rightarrow O + O_3$, lies close in energy to $v = 25$ of O_2. Realizing that the potential surface used in the theoretical calculations did not allow ozone formation added further weight to the hypothesis of reaction above $v = 25$. Further indirect evidence came by preparing states above $v = 25$ and probing lower vibrational levels. These experiments showed that the prepared $v = 25$ population was not completely accounted for in lower vibrational states, indicating a "dark channel" consistent with reaction.[80]

The possibility that highly vibrationally excited O_2 can be formed in the atmosphere and lead to ozone formation has implications for the stratospheric ozone budget. The reaction cycle,

$$O_3 + h\nu \rightarrow O(^3P) + O_2(\chi^3 E_g^-, v \gg 0) \quad \text{(R1)}$$

$$O_2(\chi^3 E_g^-, v \gg 0) + O_2 \rightarrow O(^3P) + O_3 \quad \text{(R2)}$$

$$2O(^3P) + 2O_2 \rightarrow 2O_3 \quad \text{(R3)}$$

is a net ozone production mechanism. Furthermore, inclusion of these reactions in standard stratospheric ozone models gave improved agreement with observation.[76] This provided a potential solution to the so-called "ozone deficit problem",[81−83] which refers to the difficulty in accounting for the stratospheric ozone altitude profile.

While early theoretical studies gave excellent agreement with experiment below $v = 25$; more recently, theoretical studies of the potential energy hypersurface of (R2) and dynamical studies of the reaction have failed to confirm efficient production of ozone from collisions of $O_2(\chi^3 E_g^-, v > 25)$ with O_2.[76,84−87] Even more disturbing, no quantitatively accurate alternative arises from theory that accounts for the enhanced vibrational relaxation above $v = 25$.[88]

Very recently, new evidence has been found that may help explain the difference between theory and experiment. Figure

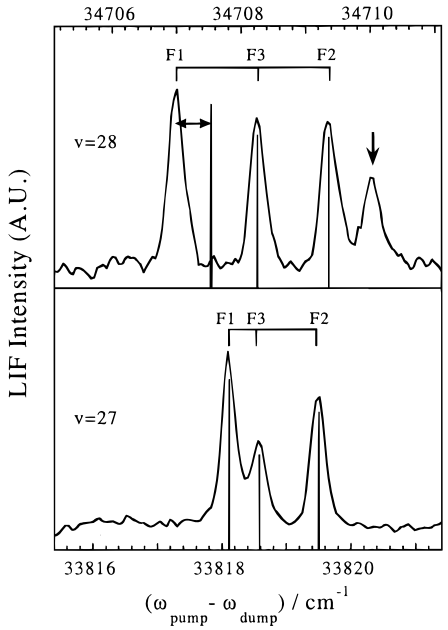

Figure 16. The first detected perturbation in the O_2 $X^3\Sigma_g^-$ ground state appears for $v = 28$. We show the SEP spectra of the $N = 5$ rigid rotor levels of $v = 27$ (bottom) and $v = 28$ (top). Both spectra show the assignment of the transitions between identical spin components (F1, $J = N + 1$; F2, $J = N$; F3, $J = N - 1$), and a calculated stick spectrum for the expected peak positions of the different transitions. Agreement between calculated and measured transition frequencies is excellent for $v = 27$ as well as for the F2 and F3 component of $v = 28$. The F1 component of the $v = 28$ spectrum, however, is shifted by $\sim$0.6 cm^{-1}. This shift is caused by a perturbing $b^1\Sigma_g^+$($v = 19$, $J = N = 6$) level, which appears as an "extra" peak (indicated with the vertical arrow). This perturbation suggests that collisions of highly vibrationally excited O_2 with O_2 may pass over more than one potential energy surface.

16 shows high resolution SEP spectra of highly vibrationally excited O_2($v = 27$ and 28).[89] Both spectra show the spin fine structure of the two $N = 5$ rigid rotor states. The two stick spectra are calculated from high-precision molecular constants that include vibration−rotation−spin interactions up to third order in perturbation theory. The calculation agrees very well with experiment for $v = 27$ and for the F_2($J = 5$) and F_3($J = 4$) components of $v = 28$. The F_1($J = 6$) feature of the $v = 28$ spectrum is, however, shifted $\sim$0.6 cm^{-1} to the red of its expected position and an "extra" peak (marked with an arrow) appears in the spectrum. This is clear evidence of an interaction between and mixing of two zeroth-order $J = 6$ states, which are nearly isoenergetic.

A complete deperturbation analysis was performed, and the perturber was assigned to O_2($b^1\,E_g^+$, $v = 19$). Using precise spectroscopic data for high vibrational states of both electronic states, a crossing between the $\chi^3\,E_g^-$ and $b_1\,E_g^+$ potentials r was found. The position of this crossing is somewhat higher in energy and more extended in bond length than the outer classical turning points of the high vibrational states of O_2 known to participate in the dark channel mentioned above.

Nevertheless, it is possible that this curve crossing is significantly stabilized by the presence of another O_2 molecule. The dissociation energy of O_2, D_0(O−O) = 493.6 kJ/mol, is substantially stabilized in the presence of another O_2 molecule, $O_2 + O_2 \rightarrow O + O_3$, 409 kJ/mol. Since both X and b state dissociation correlates to ground state O atoms, it is possible that the b−X curve crossing is also stabilized in the entrance channel of the reaction. If the energy of the curve crossing found in the RKR analysis (472 kJ/mol) was stabilized by the same amount as O_2 dissociation, vibrational states above $v = 25$ would possess enough energy to reach the crossing. This is precisely the threshold where enhanced vibrational removal is observed experimentally. These results suggest that the collision dynamics of highly vibrationally excited $O_2(\chi^3\,E_g^-)$ may involve participation of excited surfaces. Since none of the theoretical calculations have yet tried to describe the electronically adiabatic effects, this would explain why the beautiful agreement (shown in Figure 16) for vibrational states below $v = 25$ is not seen at higher energies. Determining the atmospheric fate of highly vibrationally excited O_2 may well require a deeper understanding of collisional processes occurring on several potential surfaces.

4. The Future

The PUMP−DUMP−PROBE method has given us an opportunity to examine many aspects of the behavior of highly vibrationally excited molecules, and much of this work has been (at least briefly) described in this article. Up to now, research in this field has been quite open-ended. Nearly everywhere we have looked, we have found new and unusual behavior. A great deal of effort is still required before this new phenomenology can be thoroughly understood. It is fair to ask, "now that we have some idea about what these species can do, where do we go from here knowing what we know?"

There are two possible approaches that both have substantial merit. First, we have identified a number of interesting phenomena that seem to be characteristic of super-excited molecules. These include multiquantum vibrational energy transfer at surfaces, near resonant V−V energy transfer, and nonadiabatic interactions between vibrational and electronic degrees of freedom. It is logical and valuable to delve into these and try to understand them at a deeper level.

Particularly fascinating is the study of vibrational energy transfer and reactivity at surfaces. For example, high-resolution translation and angular distribution measurements of scattered molecules resulting from multiquantum relaxation at surfaces could distinguish the "transient negative ion" mechanism from the "excited NO_2 adsorbate" mechanism mentioned in section 3.4. Modifications to the surface, for example using Gold where oxidation is unimportant, would give useful mechanistic information. Orientation studies, controlling whether the N-side or the O-side of the molecule interacts with the surface first, would also be diagnostic. Experiments on molecules with negligible electron affinity, for example, using overtone pumping of HCl, would also be quite interesting.

V−V transfer appears to be very important for relaxation of super-excited molecules. The observation that 2−1 resonances are as important as 1−1 resonances was unexpected. This suggests 3−1 resonances may also be important. This could be explored quite easily in crossed beams similar to section 3.3. For example, high vibrational states of NO are in 3−1 resonance with the HF fundamental. Using velocity map imaging methods,[90] one could also measure the angular distributions of the scattered molecules. This would help show if the details of the V−V mechanism are different for 2−1 and 3−1 resonances in comparison to the more common 1−1.

The second approach seeks to open entirely new areas of phenomenology. Investigating the chemical behavior of highly vibrationally excited molecules larger than diatomics is such an undertaking. If NO and O_2 are "scalars", where the magnitude of the vibrational excitation can be varied, polyatomic molecules are "vectors", where both the magnitude (degree of excitation) and direction (vibrational character) may be varied. This provides an inherently rich field of inquiry. It is now known

that regular vibrational states with ordered vibrational motion do persist at high energies and many of these have been identified, for example, in acetylene.[91] The collisional properties of such molecules are far from obvious. Is rotational energy transfer still more probable than vibrational energy transfer? Can the ordered motion of these vibrationally excited states be used to promote chemical reactions, or does order decay to chaos faster than reaction can occur? Can different kinds of vibration be excited to influence the outcome of a chemical reaction? What kind of chemical specificity, if any, do the "statistical" vibrational states exhibit? Some of these issues have troubled physical chemists for years, but it is only now that we are reaching the level of technical sophistication necessary to perform detailed experimental studies. The future is bright!

Acknowledgment. The work described in this article was supported by several funding agencies. These include the National Science Foundation under Grants CHE-8957978, CHE-9318885, ATM-8922214, ATM-9300074, and ATM-9633002, the Department of Energy Office of Basic Energy Sciences under Grant DE-FG03-94ER14492, and the Airforce Office of Scientific research under Grant F49620-95-1-0234. The work would not have been possible without the assistance of the Santa Barbara Laser Pool funded under NSF group instrumentation Grant CHE-9413030. We thank Prof. Paul Houston for help in the preparation of Figure 14 and Prof. Ramon Hernandez-Lamoneda for help in the preparation of Figure 15.

References and Notes

(1) Zewail, A. H.; Casati, G.; Rice, S. A.; Chergui, M.; Tannor, D. J.; Kobayashi, T.; Rabitz, H. *Adv. Chem. Phys.* **1997**, *101*, 3.
(2) Moore, G. B.; Smith, I. W. M. *J. Phys. Chem.* **1996**, *100*, 12848.
(3) Alagia, M.; Balucani, N.; Casavecchia, P.; Stranges, D.; Volpi, G. G. *J. Chem. Soc., Faraday Trans.* **1995**, *91*, 575.
(4) Alexander, A. J.; Brouard, M.; Kalogerakis, K. S.; Simons, J. P. *Chem. Soc. Rev.* **1998**, *27*, 405.
(5) Manolopoulos, D. E.; Stark, K.; Werner, H.-J.; Arnold, D. W.; Bradforth, S. E.; Neumark, D. M. *Science* **1993,** *262*, 1852.
(6) Clary, D. C. *Science* **1998**, *279*, 1879.
(7) Truhlar, D. G.; Garrett, B. C.; Klippenstein, S. J. *J. Phys. Chem.* **1996**, *100*, 12771.
(8) Polanyi, J. C. *Angew. Chem.* **1987**, *26*, 952.
(9) Lee, Y. T. *Angew. Chem.* **1987**, *26*, 939.
(10) Herschbach, D. R. *Angew. Chem.* **1987**, *26*, 1221.
(11) Bergmann, K.; Theuer, H.; Shore, B. W. *Rev. Mod. Phys.* **1998**, *70*, 1003.
(12) Hamilton, C. E.; Kinsey, J. L.; Field, R. W. *Annu. Rev. Phys. Chem.* **1986**, *37*, 493.
(13) Crim, F. F. *J. Phys. Chem.* **1996**, *100*, 12725.
(14) Yang, X.; Wodtke, A. M. *Int. Rev. Phys. Chem.* **1993**, *12*, 123.
(15) Yang, X. M.; Rogaski, C. A.; Wodtke, A. M. *J. Opt. Soc. Am.* **1990**, *B7*, 1835.
(16) Yang, X. M.; Rogaski, C. A.; Wodtke, A. M. *J. Chem. Phys.* **1990**, *92*, 2111.
(17) Jonas, D. M.; Yang, X. M.; Wodtke, A. M. *J. Chem. Phys.* **1992**, *97*, 2284.
(18) Chen, Y. T.; Watt, D. M.; Field, R. W.; Lehmann, K. K. *J. Chem. Phys.* **1990**, *93*, 2149.
(19) Ishikawa, H.; Nagao, C.; Mikami, N.; Field, R. W. *J. Chem. Phys.* **1997**, *106*, 2980.
(20) Ishikawa, H.; Chen, Y. T.; Ohshima, Y. Y.; Wang, J.; Field, R. W. *J. Chem. Phys.* **1996**, *105*, 7383.
(21) Field, R. W.; O'Brien, J. P.; Jacobson, M. P.; Solina, S. A. B.; Polik, W. F.; Ishikawa, H. *Adv. Chem. Phys.* **1997**, *101*, 463.
(22) Sinha, A.; Hsiao, M. C.; Crim, F. F. *J. Chem. Phys.* **1991**, *94*, 4928.
(23) Sinha, A.; Thoemke J. D.; Crim, F. F. *J. Chem. Phys.* **1992**, *96*, 372.
(24) Michelsen, H. A.; Rettner, C. T.; Auerbach, D. J. In *Surface Reactions*; Madix, R. J., Ed.; Springer-Verlag: Berlin, 1993; p 186.
(25) Flynn, G. W.; Parmenter, C. S.; Wodtke, A. M. *J. Phys. Chem.* **1996**, *100*, 12817.
(26) Dai, H. L. Highly Excited Molecules. *ACS Symp. Ser.* **1997**, *678*, 266.
(27) Yang, X.; Wodtke, A. M. *J. Chem. Phys.* **1990**, *92*, 116.
(28) Drabbels, M.; Wodtke, A. M. Highly Excited Molecules. *ACS Symp. Ser.* **1997**, *678*, 173.
(29) Krätzchmar, O.; Selzle, H. L.; Schlag, E. W. *J. Phys. Chem.* **1994**, *98*, 3501.
(30) Zhang, Q.; Kandel, S. A.; Wasserman, T. A. W.; Vaccaro, P. H. *J. Chem. Phys.* **1992**, *96*, 1640.
(31) Northrup, F. J.; Sears, T. J. *Annu. Rev. Phys. Chem.* **1992**, *43*, 127.
(32) Kittrell, C.; Abramson, E.; Kinsey, J. L.; Mcdonald, S. A.; Reisner, D. E.; Field, R. W.; Katayama, D. H. *J. Chem. Phys.* **1981**, *75*, 2056.
(33) Choi, Y. S.; Moore, C. B. *J. Chem. Phys.* **1989**, *90*, 3875.
(34) Meinel, A. B. *Astrophys. J.* **1950**, *111*, 555.
(35) Meinel, A. B. *Astrophys. J.* **1950**, *112*, 120.
(36) Wise, J. O.; Carovillano R. L.; Carlson H. C.; Roble R. G.; Adlergolden, S.; Nadile R. M.; Ahmadjian, M. *J. Geophys. Res.* **1995**, *100*, 21357.
(37) Sharma, R. D.; Dothe, H.; von Esse, F.; Kharchenko, V. A.; Sun, Y.; Dalgarno, A. *J. Geophys. Res.* **1996**, *101*, 19707.
(38) Sharma, R. D.; Dothe, H.; Duff, J. W. *J. Geophys. Res., Space* **1998**, *103*, 14753.
(39) Drabbels, M.; Wodtke, A. M. *J. Chem. Phys.* **1997**, *106*, 3024.
(40) Rydberg, R. *Ann. Phys.* **1931**, *73*, 376.
(41) Klein, O. *Z. Phys.* **1932**, *76*, 226.
(42) Rees, A. L. G. *Proc. Phys. Soc., London* **1947**, *A59*, 998.
(43) Nelson, D. D.; Schiffman, A.; Nesbitt, D. J.; Orlando, J. J.; Burkholder, J. B. *J. Chem. Phys.* **1990**, *93*, 7003.
(44) Rawlins, W. T.; Fraser, M. E.; Miller, S. M.; Blumberg, W. A. M. *J. Chem. Phys.* **1992**, *96*, 7555.
(45) Rawlins, W. T.; Person, J. C.; Fraser, M. E.; Miller, S. M.; Blumberg, W. A. M. *J. Chem. Phys.* **1998**, *109*, 3409.
(46) Yang, X.; Kim, E. H.; Wodtke, A. M. *J. Chem. Phys.* **1992**, *96*, 5123.
(47) Drabbels, M.; Wodtke, A. M.; Yang, M.; Alexander, M. H. *J. Phys. Chem.* **1997**, *101*, 6463.
(48) van Leuken, J. J.; van Amerom, F. H. W.; Bulthuis, J.; Snijders, J. G.; Stolte, S. *J. Phys. Chem.* **1995**, *99*, 15573.
(49) Rettner, C. T.; Auerbach, D. J.; Michelsen, H. A. *Phys. Rev. Lett.* **1992**, *68*, 2547.
(50) Yang, X.; Kim, E. H.; Wodtke, A. M. *J. Chem. Phys.* **1990**, *93*, 4483.
(51) Schwartz, R. N.; Slawsky, Z. I.; Herzfeld, K. F. *J. Chem. Phys.* **1952**, *20*, 1591.
(52) Chaban, G.; Gordon, M. S.; Nguyen, K. A. *J. Phys. Chem.* **1997**, *101A*, 4283.
(53) Price, J. M.; Mack, J. A.; Rogaski, C. A.; Wodtke, A. M. *Chem. Phys.* **1993**, *175*, 83.
(54) Mack, J. A.; Mikulecky, K.; Wodtke, A. M. *J. Chem. Phys.* **1996**, *105*, 4105.
(55) Mahan, B. H. *J. Chem. Phys.* **1967**, 4698.
(56) Sharma, R. D.; Brau, C. A. *J. Chem. Phys.* **1969**, *50*, 924.
(57) Jeffers, W. Q.; Kelley, J. D. *J. Chem. Phys.* **1971**, *55*, 4433.
(58) Stephenson, J. C.; Moore, C. B. *J. Chem. Phys.* **1972**, *56*, 1295.
(59) Drabbels, M.; Wodtke, A. M. *J. Chem. Phys.* **1998**, *109*, 355.
(60) Herzberg, G. *Infrared and Raman Spectra*; Van Nostrand: Princeton, 1945.
(61) Asscher, M.; Guthrie, W. L.; Lin, T.-H.; Somorjai, G. A. *Phys. Rev. Lett.* **1982**, *49*, 76.
(62) Mantell, D. A.; Maa, Y.-F.; Ryali, S. B.; Haller, G. L.; Fenn J. B. *J. Chem. Phys.* **1983**, *78*, 6338.
(63) Rettner, C. T.; Fabre, F.; Kimman, J.; Auerbach, D. J. *Phys. Rev. Lett.* **1985**, *55*, 1904.
(64) Kay, B. D.; Raymond, T. D.; Coltrin, M. E. *Phys. Rev. Lett.* **1987**, *59*, 2792.
(65) Hodgson, A.; Samson, P.; Wight, A.; Cottrell, C. *Phys. Rev. Lett.* **1997**, *78*, 963.
(66) Rettner, C. T.; Auerbach, D. J.; Michelsen, H. A. *Phys. Rev. Lett.* **1992**, *68*, 2547.
(67) Persson, B. N. J.; Gadzuk, J. W. *Surf. Science* **1998**, *410*, L779.
(68) Persson, B. N. J.; Avouris, P. *Surf. Science* **1997,** *390*, 45.
(69) Matloob, M. H.; Roberts, M. W. *Phys. Scr.* **1977**, *16*, 420.
(70) Watts, E. K.; Siders, J. L. W.; Sitz, G. O. *Surf. Sci.* **1997**, *374*, 191.
(71) Habraken, F. H. P. M.; Kieffer, E. P.; Bootsma, G. A. *Surf. Sci.* **1979** , *83*, 45.
(72) Hou, H.; Huang, Y.; Rettner, C. T.; Gulding, S. J.; Auerbach, D. J.; Wodtke, A. M. *J. Chem. Phys.* **1999** *110*, 10660.
(73) Rettner, C. T.; Pfnhr, H. E.; Stein, H.; Auerbach, D. J. *J. Vac. Sci. Technol.* **1988**, *A6*, 899.
(74) Gostein, M.; Parhikhteh, H.; Sitz, G. O. *Phys. Rev. Lett.* **1995**, *75*, 342.
(75) Hou, H.; Huang, Y.; Rettner, C. T.; Gulding, S. J.; Auerbach, D. J.; Wodtke, A. M. *Science*, in press.
(76) Miller, R. L.; Suits, A. G.; Houston, P. L.; Toumi, R.; Mack, J. A.; Wodtke, A. M. *Science* **1994**, *265*, 1831.

(77) Heck, A. J. R.; Chandler, D. W. *Annu. Rev. Phys. Chem.* **1995**, *46*, 335.
(78) Hernandez-Lamoneda, R.; Toumi, R.; Clary, D. C. *J. Chem. Phys.* **1995**, *102*, 9544.
(79) Rogaski, C. A.; Price, J. M.; Mack, J. A.; Wodtke, A. M. *Geophys. Res. Lett.* **1993**, *20*, 2885.
(80) Rogaski, C. A.; Mack, J. A.; Wodtke, A. M. *Faraday Discuss. (Atmospheric Chemistry)* **1996**, *100*, 229.
(81) Khosravi, R.; Brasseur, G. P.; Smith, A. K.; Rusch, D. W.; Waters, J. W.; Russell, J. M., III *J. Geophys. Res.* **1998**, *103*, 16203.
(82) Siskind, D. E.; Connor, B. J.; Eckman, R. S.; Remsberg, E. E.; Tsou, J. J.; Parrish, A. *J. Geophys. Res.* **1995**, *100*, 11191.
(83) Eluszkiewicz, J.; Allen, M. *J. Geophys. Res.* **1993**, *98*, 1069.
(84) Hernandez-Lamoneda, R.; Hernández, M. I.; Carmona-Novillo, E.; Campos-Martínez, J.; Echave, J.; Clary, D. C. *Chem. Phys. Lett.* **1997**, *276*, 152.
(85) Lauvergnat, D.; Clary, D. C. *J. Chem. Phys.* **1998**, *108*, 3566.
(86) Varandas, A. J. C.; Wang, W. *Chem. Phys.*,**1997**, *2*, 167.
(87) Campos-Martinez, J.; Carmona-Novilloa, E.; Echave, J.; Hernández, M. I.; Hernández-Lamoneda, R.; Palma, J. *Chem. Phys. Lett.* **1998**, *289*, 150.
(88) Jongma, R. T.; Shi, S.; Wodtke, A. M. *J. Chem. Phys.*, submitted.
(89) Eppink, A. T. J. B.; Parker, D. H. *Rev. Sci. Instrum.* **1997**, *68*, 3477.
(90) Jacobson, M. P.; O'Brien, J. P.; Silbey, R. J.; Field, R. W. *J. Chem. Phys.* **1998**, *109*, 121.